J. Inst. Electrostat. Jpn.
論　　文
静電気学会誌，**49**, 6（2025）200-205

Analysis of Nitrogen Fixation Characteristics in Water with Plasma in Underwater Air Bubbles

Hailiang GAO*, Wangke ZHANG* and Nozomi TAKEUCHI*, 1

（Received March 3, 2025; Accepted July 1, 2025）

We systematically investigated the generation characteristics of active species in both gas and liquid phases during nitrogen fixation process using plasma in under water air bubbles. The results demonstrated that a higher gas flow rate leads to lower energy cost and the lowest energy cost of 27 MJ/mol-N was achieved at a gas flow rate of 1.5 L/min with a driving frequency of 100 kHz. Additionally, in gas humidification experiments, excessive water vapor was found to suppress the production of reactive nitrogen species. A gas recirculation experiment further showed that recirculating gas can effectively reduce the energy cost. This study provides valuable insights into optimizing plasma discharge parameters for improved energy efficiency in nitrogen fixation, contributing to the development of a more sustainable and environmentally friendly plasma-based approach.

1. Introduction

Nitrogen is a fundamental element of all forms of life, serving as a critical component of amino acids, proteins, nucleic acids, and more. For example, the human's body need 1－2 g of protein per kilo gram of weight per day to live[1]. The earth atmosphere contains an abundant supply of nitrogen, with 78.08％ of the air composed of nitrogen molecules（N_2）. However, most organisms can't utilize nitrogen directly. Only plants and certain bacteria can transform free nitrogen into amino acids that can be used for biological processes. Because of the high strength of N≡N bonds, it is difficult to convert the nitrogen into simple compounds such as ammonia or nitrogen dioxide. Therefore, various methods have been explored to achieve nitrogen fixation. Among them, Haber–Bosch process remains the primary method for industrial nitrogen fixation. In addition, the commercial production of reactive nitrogen-based chemicals mainly relies on NH_3 produced through the Haber–Bosch process as a foundation[2]. However, the Haber–Bosch process faces growing challenge because of high energy consumption and environmental impact. It accounts for 1－2％ of global energy storage and emits substantial amount of CO_2. Therefore, to develop a low carbon, efficient, and economic nitrogen fixation technology has gradually become the research hotpot.

In recent year, as one of the most promising methods of nitrogen fixation, low-temperature plasma（LTP）has attracted people's attention due to its advantages of small scale, mild reaction conditions, and flexible and controllable parameters. Compared to Haber–Bosch process and Birkeland–Eyde process（an industrial method that uses electrical arcs to react N_2 with O_2 ultimately producing HNO_3 with water）, the LTP has lower energy consumption in theoretical standard, which is about 0.2 MJ/mol-N[3]. And the main methods using LTP are divided into two categories: one is the ammonia synthesis; the other is NOx synthesis or direct production of NO_2^- and NO_3^-. In 2023, Kim et al. investigated NOx synthesis from ambient air by spark discharge, which has higher energy efficiency compared to high-frequency dielectric barrier discharge because of its higher vibrational and rotational excitations and their effective utilization[4].

This study employs a discharge at a gas－liquid interface to achieve nitrogen fixation by directly generating nitrates. We used a high-frequency pulsed power supply for underwater bubble plasma discharge to study the characteristics of the resulting plasma and the formation of reactive oxygen and nitrogen species（RONS）in the gas and liquid phases.

2. Experiment

2.1 Experimental setup

The reactor for plasma in underwater air bubbles is shown in Fig.1, and the experimental set up is shown in Fig.2. In our previous studies using a similar plasma treatment system, we have found that the exhaust gas which had passed through a solution after the plasma reaction still contains a large amount of nitrogen oxides（NOx）, especially NO_2. To improve production efficiency of liquid-phase reactive nitrogen species（RNS）, this study extends the reactor height to prolong the gas dissolution time in the solution. The new reactor consists of two parts made of acrylic: a solution storage part and a high voltage（H.V.）

Keywords：plasma, RONS, energy cost

* Department of Electrical and Electronic Engineering, Institute of Science Tokyo, 2-12-1 Ookayama, Meguro-ku, Tokyo 152-8552, Japan
[1] takeuchi@ee.eng.isct.ac.jp

DOI：https://doi.org/10.34342/iesj.2025.49.6.200

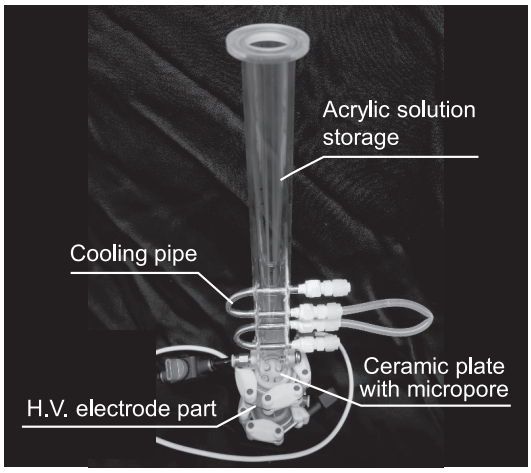

Fig.1 Image of reactor.

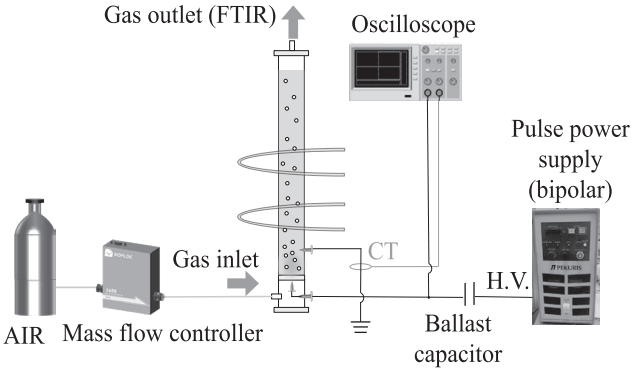

Fig.2 Experimental setup.

electrode part. A 1 mm-thick ceramic plate（Kurosaki Harima, 99.7% alumina）with a micropore of 0.3 mm is placed at the bottom of the solution storage. The solution storage has a height of 300 mm（that in previous studies are 120 mm）and contains a solution of 120 mL. To ensure stable discharge, a NaCl solution with a conductivity of 1000 μS/cm is used. A molybdenum electrode is positioned below the micropore, similar to our previous studies[5]. The gap between the electrode tip and the micropore is 1 mm. Air is introduced into the reactor through a gas inlet at the H.V. electrode part and flows through the micropore, generating bubbles as it enters the solution. The air flow rate is precisely controlled by a mass flow controller（KOFLOC, 8700, 2SLM）. A high voltage is applied to the electrode, accompanied by a ballast capacitor, while the solution is grounded. The applied voltage is generated by using a bipolar pulse power supply（Kurita Manufacturing Co., Ltd. MPP04-A4-200）. Plasma is generated between the tip of the H.V. electrode and the bubble–solution interface. Typical voltage and current waveforms are shown in Fig.3.

All experiments were carried out at room temperature and atmospheric pressure. A cooling system was used to maintain the

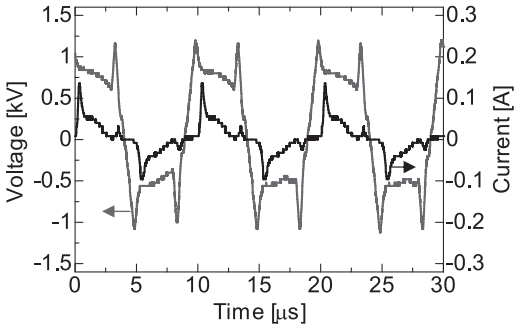

Fig.3 Typical voltage and current waveforms.

solution temperature at 20℃. Solution samples were taken every 10 min and left to stand for at least 10 min before measurement with a UV-Vis spectroscopy（JASCO, V-730）. The exhaust gas was thoroughly dried using a dehumidifier after exiting the reactor, then analyzed using FTIR spectroscopy（JASCO, FTIR-6600）.

2.2 UV-Vis measurement

Solutions treated by the plasma are quantitatively analyzed by UV-Vis spectrophotometer. The parameters of the absorbance spectrophotometer are a bandwidth of 1.0 nm, scanning speed of 200 nm/min, and data interval of 0.2 nm. The optical path length of light passing through a quartz cuvette used for the measurement was kept constant at 10 mm.

First, the transmittance of ultrapure water（T'）and the transmittance of the sample（T）are measured in the sample measurement section with respect to the background, and the transmittance spectrum is converted to absorbance Abs by the following equation:

$$\mathrm{Abs} = \log\left(\frac{T'}{T}\right) \quad (1)$$

Next, the absorption spectra are fitted using absorption spectra of various substances measured beforehand. When the optical path length is constant, there is a proportional relationship between the absorbance at a certain wavelength λ and the concentration of the target substance, so quantitative evaluation of RONS is performed by determining the concentration from the absorbance. The concentrations of RONS were obtained using the least square error fitting of the absorption spectra with the molar extinction coefficient of the individual species. The fitting analysis was performed by a standalone MATLAB application Fit（Lite）ver. 1.11 developed at Tohoku University[6,7].

2.3 Evaluation of power consumption

The experimental conditions are shown in Table 1. The power consumption（p）in the reactor was calculated by the following equation:

Table 1　Experimental conditions.

Parameters	Value
Voltage	2 kV
Ballast capacitance	25 pF
Frequency	100 kHz
Flow rate	0.1 − 1.5 L/min
Power	22 − 25 W

$$p = f\int_0^{\tau} vi\,dt \quad (2)$$

here, f is the frequency of the applied voltage, τ is the period of one cycle, and v and i are the instantaneous values of the applied voltage and current, respectively. The powers of all sets of experiments were approximately 22–25 W

3. Experimental results

3.1 Effect of gas flow rate

The concentration of the products in the solution is shown in Fig.4. The figures clearly demonstrate that the concentration of NO_3^- increases as the gas flow rate increases. In contrast, the concentration of NO_2^- decreases as the gas flow rate increases. Two main factors underlie this phenomenon. On one hand, in our previous studies, we have found that in a shorter reactor, the concentration of NO_3^- exhibits a saturation trend as the gas flow rate increases, which means that the NO_3^- concentration remains almost the same at different gas flow rates. The shorter reactor has a limited residence time of gas bubbles in the solution, which restricted the dissolution of NO_2 and causes the saturation trend in NO_3^- concentration as gas flow rate increased. On the other hand, gas-phase plasma is generated in the plasma–liquid interface, where the reactive species are transferred into the liquid by diffusion process alone. The species transfer rate can be improved by increasing the gas flow rate or by having forced convection through liquid mixing. Therefore, increasing the gas flow rate accelerates the diffusion of various active species, such as H_2O_2 and OH radical, from the gas phase to the liquid phase. This effect enhances the availability of oxidizing agents accelerating the oxidation of NO_2^-/HNO_2 to NO_3^- as shown in equations (3)–(4) [6,8]. The above factor leads to opposite variation trends for NO_3^- and NO_2^-/HNO_2.

$$HNO_2 + H_2O_2 + H^+ \rightarrow ONOOH + H_2O + H^+ \quad (3)$$

$$ONOOH \rightarrow HNO_3 \rightarrow NO_3^- + H^+ \quad (4)$$

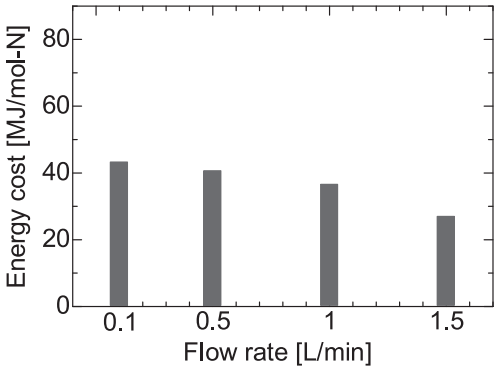

Fig.5　Energy cost with different gas flow rates.

Fig.5 shows the energy cost to produce the liquid-phase RNS. The energy cost decreased progressively with increasing gas flow rate, reaching a minimum value of 27 MJ/mol-N at 1.5 L/min. The results indicate that at similar power levels, a higher gas flow rate can effectively reduce the energy cost. However, this trend is opposite to our previous studies with the shorter reactor, where the lower gas flow rate resulted in lower energy cost. This is because the lifetime of bubbles shortens with increasing gas flow rate and dissolution time to generate liquid-phase RNS is not enough. Therefore, the gas flow rate must be coordinated with an appropriate reactor height. Under conditions with sufficient dissolution time, a higher gas flow rate can significantly reduce the energy cost.

3.2 Experiments of gas recirculation

Fig.6 shows the amount of N atoms in the solution and exhaust gas after 60 min treatment. In this experiment, the main components contained in the exhaust gas and their corresponding wavenumbers are: HNO_3 (1300 cm^{-1} and 1700 cm^{-1}), N_2O (1300 cm^{-1} and 2200 cm^{-1}), NO_2 (2900 cm^{-1} and 1600 cm^{-1}),

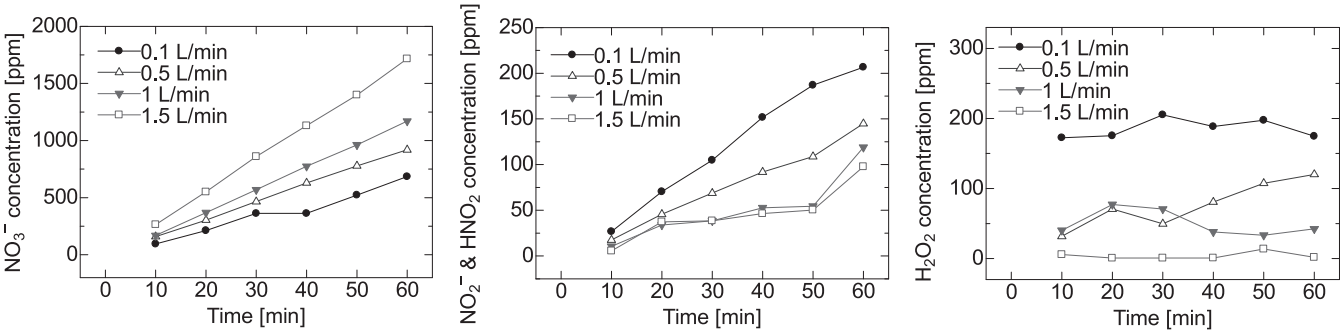

Fig.4　Products in solution with different gas flow rates.

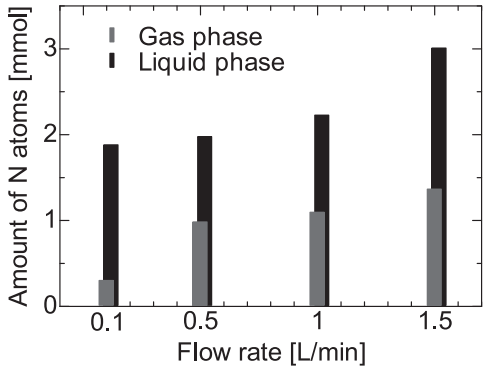

Fig.6 Amount of N atoms in solution and exhaust gas.

NO（1900 cm^{-1}), and O_3（2100 cm^{-1} and 1000 cm^{-1}). The increase in gas flow rate leads to an increase in liquid-phase products; however, there are still RNS in the exhaust gas. The amount of unabsorbed RNS increases as increasing gas flow rate. Ozone also exists in the exhaust gas with a concentration less than 30 ppm in all conditions.

To fully utilize the RNS in the exhaust gas, we conducted a closed-loop gas recirculation experiments to enhance energy efficiency and exhaust gas utilization. Based on the original setup, the recirculation system is modified by disconnecting external air and reserving 30 mL of air at the top of the reactor. A gas pump is then used to recirculate the gas. After 5–15-min discharge, the gas is recirculated through the solution for 15 min to ensure the full absorption of RNS in the gas phase. To ensure a sealed environment and accommodate the power limitations of the pump, the gas flow rate in this experiment was restricted to 0.2 L/min. However, even at a low flow rate, the gas recirculation still demonstrated good performance.

The result is shown in Fig.7. With the increase in gas recirculation time, the concentration of NO_3^- in the solution increases significantly, while the concentration of NO_2^- gradually decreases to tens of ppm. A possible reason is that some long-lived species, such as O_3 and H_2O_2, exist in the liquid phase with high stability and can persist for tens of min, continuously oxidizing NO_2^- in the liquid phase as shown in equations（3）–（5）[9].

$$NO_2^- + O_3 \rightarrow NO_3^- + O_2. \quad (5)$$

In terms of energy cost, the recirculation system consumes 32 MJ/mol-N after 15 min of discharge and 15 min of circulation, whereas the non-recirculation system requires 47 MJ/mol-N. This indicates that gas recirculation can effectively reduce the energy cost of nitrogen fixation.

3.3 Experiments of humid air

The water vapor plays a critical role in generating OH radicals,

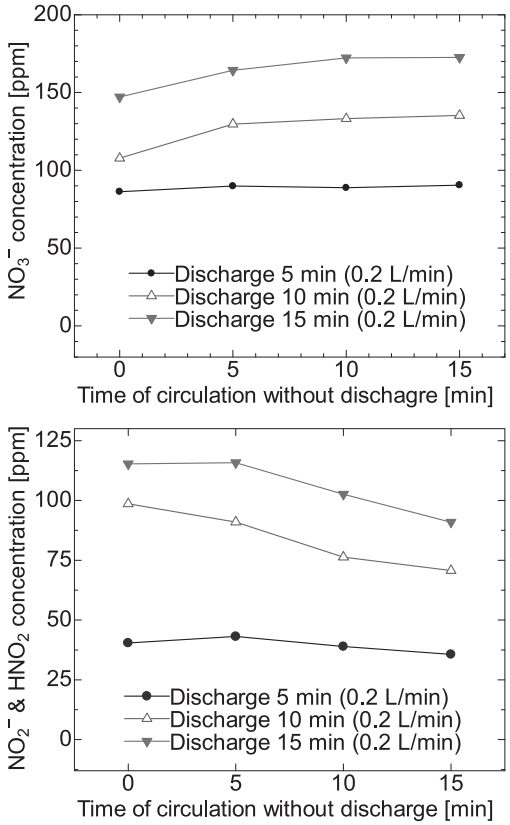

Fig.7 Products in solution with gas recirculation.

which are essential for subsequent oxidative reactions. To ensure controlled humidity levels, the inlet air was first passed through a gas washing bottle filled with hot water（80℃）to achieve vapor saturation, followed by introduction into the reactor. This setup guarantees a stable and reproducible humid environment for plasma activation. The experimental discharge parameters are same as Table 1.

The results of liquid-phase product analysis are presented in Fig.8. Compared to dry air, the yields of all detected products decreased under humid air. The trend of NO_3^- concentration as a function of gas flow rate remained consistent with previous observations, exhibiting improved efficiency at higher flow rates. However, the NO_2^- yield declined significantly, with its concentration remaining below 30 ppm in all cases except at 1.5 L/min. The observed suppression of RNS under elevated humidity conditions can be mechanistically linked to two interdependent factors. First, the introduction of water vapor through air humidification via hot water bubbling disproportionately diluted nitrogen content in the gas phase, thereby limiting RNS precursor availability. Second, heat absorption during vapor condensation reduced localized plasma temperatures through latent heat dissipation.

Consequently, the suppressed product yields under humid

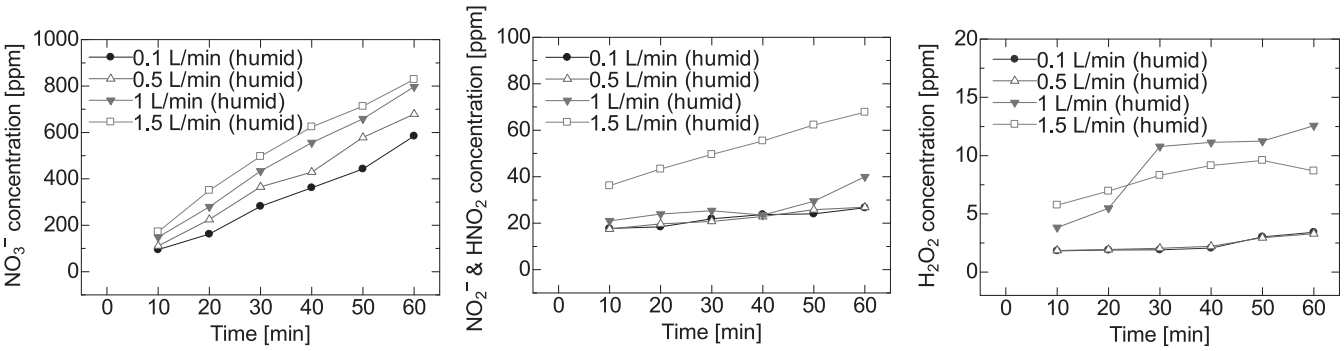

Fig.8　Products in solution with discharge with humid air.

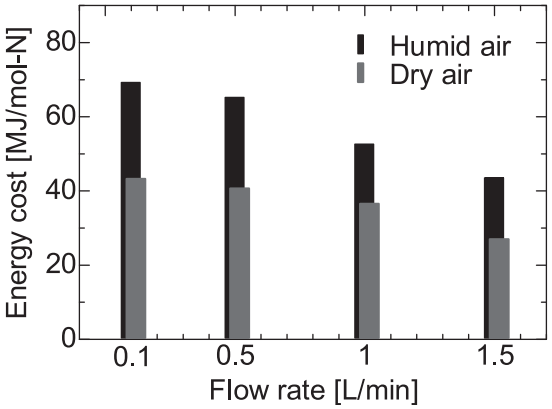

Fig.9　Comparison of energy cost in humid air and dry air.

conditions were associated with significantly higher energy cost as shown in Fig.9, which greatly exceeded those recorded in dry air experiments. Although energy cost exhibited a decreasing trend with increasing flow rate, the detrimental effects of excessive humidity overwhelmingly counteracted the benefits of gas flow rate optimization.

4. Simulation

4.1 Model description

The experiments in this study involved underwater bubble discharge, which encompasses air plasma discharge and complex gas-liquid phase interactions. The liquid-phase RONS are generated through multiple steps: (1) production of gas-phase RONS in the plasma core between the tip of the H.V. electrode and the exit of micropore, (2) diffusion of RONS into a bubble where the plasma is extended to the bubble–solution interface, and (3) dissolution of RONS into the solution. In this study, only the gas-phase plasma component in the first step was simulated. To reduce model complexity, a 0D model was employed using COMSOL Multiphysics®, focusing exclusively on the mutual reactions between ions and radicals in the gas phase. The 624 gas-phase reaction equations involved are referenced from the paper reported by Sakiyama et al.[10] Since discharges are initiated during both positive and negative polarities of the applied voltage, the electron-impact reactions are assumed to occur for 2 μs at a frequency of 200 kHz. The gas temperature is set to 300 K. The time for the simulation was 40 μs, with which the supplied gas flows from the tip of the needle and through the micropore, corresponding to the center of plasma channel. The electron energy and electron number density are set to 5 eV and 2×10^{20} m^{-3}, respectively, when discharges are initiated. The model is used to simulate the changes in RONS under different humidity levels.

4.2 Simulation results

Fig.10 shows the time development of concentrations of representative RONS. The concentration of H_2O_2 increased significantly with increasing water vapor content because more OH radicals are produced by dissociation of H_2O molecules. The concentration of O_3 decreases continuously as water vapor content increased. It can be explained that O radicals are consumed by reactions with H_2O producing OH radicals rather than the three body reaction with O_2 producing O_3 as observed in our previous study[11]. HNO_2 is the dominant species among RNS even with small water vapor content. The concentrations of HNO_2 and HNO_3 increased with increasing water vapor content while the concentrations of NO and NO_2 decreased because the oxidation of NO and NO_2 by OH radicals shown below are enhanced.

$$NO + OH + M \rightarrow HNO_2 + M \quad (6)$$

$$NO_2 + OH + M \rightarrow HNO_3 + M \quad (7)$$

Although not shown in Fig.10, the concentration of N_2O_5 was less than that of O_3.

Considering the high solubility of H_2O_2 and HNO_2, the concentrations of liquid-phase RONS would be expected to increase with higher water vapor content. However, in the experiments, the concentrations of liquid-phase RONS decreased when the air was humidified. This discrepancy between the experimental results and simulations is likely due to unstable

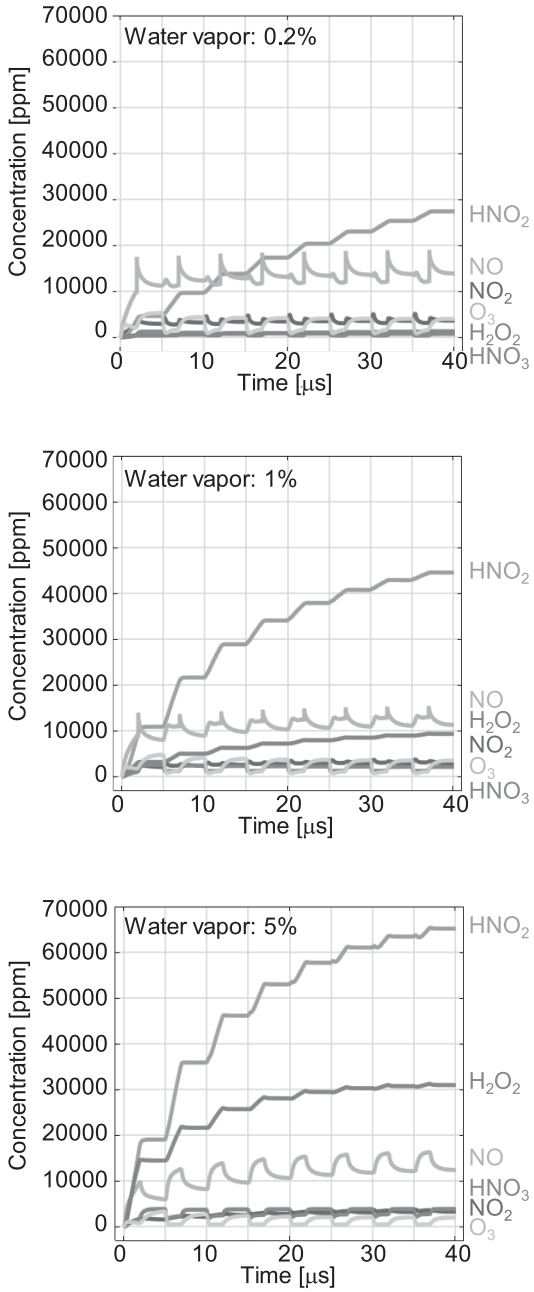

Fig.10 Time development of RONS concentration with different humidity levels.

discharge and/or a decrease in electron density and electron energy at higher water vapor levels.

5. Conclusion

In this study, we systematically investigated the generation characteristics of active species in both the gas-liquid phases by adjusting plasma discharge parameters and conditions. In the experiments on gas flow rate, the results showed that the gas flow rate can significantly affect the energy consumption, and the higher gas flow rate can get the lower the energy cost. The lowest energy cost of 27 MJ/mol-N was achieved at a flow rate of 1.5 L/min and a frequency of 100 kHz. In the gas humidification experiment, excessive water vapor was found to reduce the concentration of RNS in solution, thereby limiting efficiency. Finally, a gas recirculation experiment demonstrated that gas recirculation effectively reduced energy cost.

Numerical simulations using a 0D model revealed that the main RONS generated in the center of the plasma channel is HNO_2, and the concentrations of HNO_2 and HNO_3 increased with increasing water vapor content while the concentrations of NO and NO_2 decreased.

Acknowledgement

This work was supported by JST Grant Number JPMJPF2302.

References

1） V. Smil: Enriching the Earth, p. 9, The MIT Press（2004）
2） E. Vervloessem, Y. Gorbanev, A. Nikiforov, N. De Geyter and A. Bogaerts: Sustainable NOx production from air in pulsed plasma: elucidating the chemistry behind the low energy consumption. Green Chem., **24**（2021）916
3） N. Cherkasov, A. O. Ibhadon and P. Fitzpatrick: A review of the existing and alternative methods for greener nitrogen fixation. Chem. Eng. Process., **90**（2015）24
4） A. A. Abdelaziz, Y. Teramoto, T. Nozaki and H. H. Kim: Performance of high-frequency spark discharge for efficient NO_x production with tunable selectivity. Chem. Eng. J., **470**（2023）144182
5） R. Kazama, T. Watanabe, S. Zen and N. Takeuchi: Effect of ozone and humidity addition on hydrogen peroxide generation characteristics of plasmas in oxygen bubbles. J. Vac. Sci. Technol. A, **40**（2022）063008
6） T. Kaneko, K. Takashima and S. Sasaki: Integrated transport model for controlled delivery of short-lived reactive species via plasma-activated liquid with practical applications in plant disease control. Plasma Chem. Plasma Process., **44**（2024）1165
7） S. Sasaki: Fit（Lite）, Shota Sasaki's website.（2024）https://sites.google.com/tohoku.ac.jp/shota-sasaki/software/fit-lite
8） B. Tarabova, P. Lukes, M. U. Hammer, H. Jablonowski, T. von Woedtke, S. Reuter and Z. Machala: Fluorescence measurements of peroxynitrite/peroxynitrous acid in cold air plasma treated aqueous solutions. Phys. Chem. Chem. Phys., **21**（2019）8883
9） S. N. Pandis and J. H. Seinfeld: Sensitivity analysis of a chemical mechanism for aqueous-phase atmospheric chemistry. J. Geophys. Res., **94**（1989）1105
10） Y. Sakiyama, D. B. Graves, Huang-Wen Chang, Tetsuji Shimizu and Gregor E Morfill: Plasma chemistry model of surface microdischarge in humid air and dynamics of reactive neutral species. J. Phys. D: Appl. Phys., **45**（2012）425201
11） N. Takeuchi, Y. Ishii and K. Yasuoka: Modelling chemical reactions in dc plasma inside oxygen bubbles. Plasma Sources Sci. Technol., **21**（2012）015006